

GAINS: Gaussian-based Inverse Rendering from Sparse Multi-View Captures

Patrick Noras^{1,2} Jun Myeong Choi³ Didier Stricker^{1,2} Pieter Peers⁴ Roni Sengupta³

¹University Kaiserslautern-Landau ²German Research Center for Artificial Intelligence

³University of North Carolina at Chapel Hill ⁴College of William & Mary

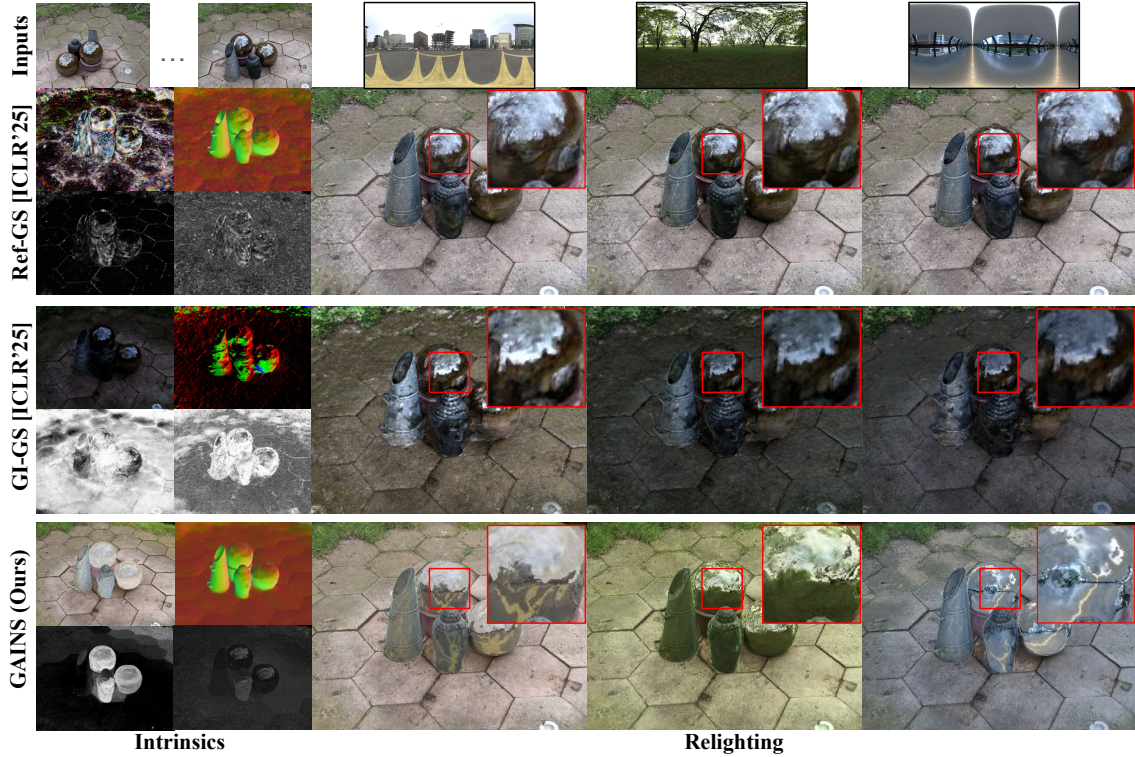


Figure 1. We introduce **GAINS**, GAussian-based INverse rendering from Sparse multi-view captures, which synergizes learning-based priors related to monocular depth/normal, segmentation, intrinsic image decomposition (IID), and diffusion, to better disambiguate reflectance from lighting, leading to better intrinsics, novel view synthesis and relighting compared to existing state-of-the-art approaches such as Ref-GS [36] and GI-GS [3]. Prior methods often overfit diffuse (e.g., missing yellow reflection from the ground in the first relighting example for GI-GS) and/or specular reflections (e.g., for both Ref-GS and GI-GS the reflected details remain unchanged under different lighting conditions). In contrast, **GAINS** improves estimation of material properties leading to better relighting in novel views.

Abstract

Recent advances in Gaussian Splatting-based inverse rendering extend Gaussian primitives with shading parameters and physically grounded light transport, enabling high-quality material recovery from dense multi-view captures. However, these methods degrade sharply under sparse-view settings, where limited observations lead to severe ambiguity between geometry, reflectance, and lighting. We introduce **GAINS** (Gaussian-based Inverse rendering from Sparse multi-view captures), a two-stage inverse rendering framework that leverages learning-based priors to stabi-

lize geometry and material estimation. **GAINS** first refines geometry using monocular depth/normal and diffusion priors, then employs segmentation, intrinsic image decomposition (IID), and diffusion priors to regularize material recovery. Extensive experiments on synthetic and real-world datasets show that **GAINS** significantly improves material parameter accuracy, relighting quality, and novel-view synthesis compared to state-of-the-art Gaussian-based inverse rendering methods, especially under sparse-view settings. Project page: <https://patrickbail.github.io/gains/>

1. Introduction

Inverse rendering (IR) aims to recover the intrinsic 3D properties of a scene (*i.e.*, geometry, material properties, and lighting) from multi-view images. IR serves as a key step toward physically grounded 3D scene understanding in many downstream applications such as novel-view synthesis, relighting, material and shape editing, etc. Over the past decades, inverse rendering has seen remarkable progress, evolving from early methods [24, 25, 38] that use simple intrinsic representations such as surface normals, albedo, and spherical harmonics lighting, to modern approaches that employ rich and realistic intrinsic representations such as 3D Gaussian primitives, physically-based BRDFs, and realistic illumination [5, 6, 14, 16, 18, 28, 31, 41]. Similarly, the scope of inverse rendering has broadened from simple, controlled objects like faces to complex real-world scenes containing intricate geometry and diverse materials.

Despite these advances, scaling inverse rendering from simple objects to complex scenes with intricate details typically requires dense multi-view captures that provide strong geometric and photometric constraints that help disambiguate material properties, lighting, and shape, all of which are entangled in the image formation process. However, when viewpoints are sparse, these constraints weaken, leading to overfitting and degraded performance. In such settings, existing methods often fail to recover accurate intrinsic properties, producing inconsistent material and lighting estimates. Moreover, traditional smoothness priors are inadequate for resolving the albedo-lighting ambiguity, resulting in poor novel-view synthesis (NVS) and relighting.

To address these challenges, we propose GAINS (GAussian-based INverse rendering from Sparse multi-view captures), a novel inverse rendering framework designed to operate robustly under sparse-view settings. We focus on a Gaussian splatting based framework since state-of-the-art approaches [3, 8, 36] found Gaussian splatting to be more effective for inverse rendering both in terms of quality and efficiency. GAINS follows the standard two-stage inverse rendering pipeline, where we first estimate geometry (Stage I), followed by an estimation of material properties and lighting (Stage II). Geometry estimation forms the foundation of physically-based rendering, and thus, high-quality geometry is crucial for accurate material and lighting recovery. In Stage I, we leverage learning-based priors from monocular depth and normal prediction networks as well as latent diffusion models, drawing inspiration from recent progress in sparse-view Gaussian-based reconstruction methods [34, 35], as detailed in Sec. 4. However, the primary contribution of GAINS lies in Stage II, where we introduce three complementary learning-based priors: (1) A *segmentation guidance* that enforces multi-view consistency and reduces noise in material maps. However, segmentation guidance lacks intrinsic

knowledge of surface reflectance, limiting its generalization to novel views and lighting conditions; (2) An *Intrinsic Image Decomposition (IID) prior*, implemented using a state-of-the-art intrinsic image decomposition network, that provides a strong initialization for albedo, at the cost of poor cross-view consistency and weak generalization; and (3) a *latent diffusion prior* that offers strong generalization capabilities. However, the latent diffusion prior struggles with material consistency and multi-view consistency. Only by combining all three complementary priors (Sec. 5), GAINS recovers robust material properties and lighting while achieving stable novel-view synthesis and relighting, even under extreme sparse input conditions.

We conduct extensive experiments on two synthetic benchmarks (TensorIR [10], which provides ground-truth albedo and relighting supervision, and Syn4Relight [44], which additionally includes ground-truth roughness), as well as one real-world dataset [29]. GAINS consistently outperforms state-of-the-art Gaussian-based inverse rendering methods across geometry and material estimation tasks. The improvements are especially pronounced under sparse-view conditions, though our method also achieves competitive results with dense inputs. We further perform detailed ablation studies to analyze the contributions of each prior and demonstrate how their combination yields the most robust and physically consistent inverse rendering results.

2. Related Work

Inverse Rendering (IR) decomposes images into geometry, material properties, and illumination. Classical methods estimate surface shape and spatially varying material properties from controlled captures using analytic BRDF models and global illumination optimization [4, 23, 33]. With the advent of learning-based scene representations such as NeRF [19], neural IR frameworks [10, 27, 32, 39, 43] integrate simplified BRDF and lighting models to recover intrinsic scene parameters from multi-view inputs. Notably, NeRFactor [43] estimates shape, materials, and lighting under unknown illumination using smoothness and BRDF priors, while GaNI [32] and related work jointly optimize geometry and material parameters with near-field lighting and neural radiance caching.

Inverse Rendering with Gaussian Splatting. Recently, 3D Gaussian Splatting (3DGS) [13] emerged as an efficient explicit radiance representation, which subsequently has been extended to IR [3, 9, 15, 26, 36]. GaussianShader [9] augments Gaussian primitives with BRDF parameters, while Ref-GS [36] and GI-GS [3] integrate physically-based rendering (PBR) with deferred shading and ray tracing. While Gaussian splatting based IR frameworks provides higher efficiency and fidelity than neural implicit representations, they assume dense multi-view captures and/or object-centric settings, making them less prac-

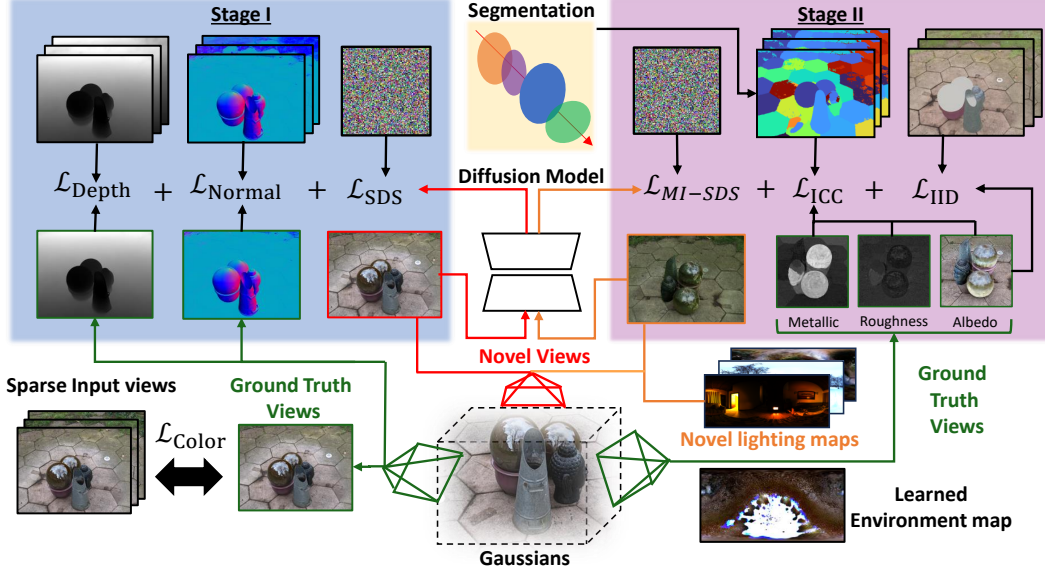


Figure 2. **GAINS** follows a two-stage inverse rendering pipeline: Stage I reconstructs geometry, and Stage II estimates material parameters and lighting. In Stage I, we enhance geometry using learning-based priors from monocular depth, normal, and diffusion predictors. In Stage II, we introduce three complementary priors: segmentation, intrinsic image decomposition (IID), and diffusion, to improve material estimation, novel-view synthesis, and relighting. Each prior provides distinct benefits: segmentation boosts cross-view consistency of specular parameters but degrades albedo; IID improves albedo accuracy but remains view-inconsistent; diffusion enhances generalization to novel view and relighting but lacks material consistency. **GAINS** integrates these priors to achieve stable, high-quality estimated material properties, leading to better relighting under novel views.

tical for real-world sparse-view scenarios.

Inverse Rendering with Sparse Views. Earlier approaches for sparse-view or single-view IR rely on learned priors from synthetic data [14, 24, 25] without explicit geometric and light-transport modeling leading to poor generalization to complex real world scenes. Recent works like RelitLRM [42] leverage Large Reconstruction Models (LRMs) and generative priors for object relighting, but they can not estimate intrinsic components (*e.g.*, material properties), nor do they generalize to complex real-world scenes.

Recent approaches for shape reconstruction from sparse views using NeRF- or 3DGS-based representations increasingly leverage learning-based priors, such as monocular depth, normal, or diffusion-based guidance [8, 30, 34, 35, 45], demonstrating that combining learned priors with explicit geometric modeling leads to significant performance gains. However, a sparse-input inverse rendering framework that jointly integrates such learning-based priors with explicit shape representations and physically based rendering remains largely unexplored, which our work addresses.

3. Overview

Our goal is to reconstruct robust and accurate geometry and material properties from a sparse set of captured RGB images $\{I_i\}_{i=1}^N$ (with N as low as 4-16 views) under known camera intrinsics and extrinsics $C_i = \{K_i, R_i, t_i\}$. Our pipeline builds on 2D Gaussian Splatting (2DGS) [7], and adapts it for robust Inverse Rendering (IR) from sparse input

views. We opt for 2DGS over 3D Gaussian Splatting [13] due to its more accurate geometry reconstruction which is essential for accurate material property estimation.

Scene representation. As in 2DGS, we parameterize the geometry as: $\mathcal{G} = \{\mu_j, S_j, R_j, \sigma_j\}_{j=1}^M$, where μ_j describes the 3D position of each primitive, along with opacity σ_j , scaling vector S_j and rotation matrix R_j ; the surface normal n_j is also determined by R_j .

Material and lighting representation. Following previous Gaussian splatting-based IR methods [3, 26, 36], we use a physically-based rendering (PBR) deferred shading approach. We employ the simplified Disney BRDF model [1] and store for each Gaussian primitive the corresponding BRDF parameters: $\mathcal{M} = \{\mathbf{a}_j, r_j, m_j\}_{j=1}^M$, where $\mathbf{a}_j \in [0, 1]^3$ is the albedo, $r_j \in [0, 1]$ the roughness and $m_j \in [0, 1]$ the metallicity. For efficiency, we employ the split-sum approximation [11] to model the diffuse and specular surface reflectance:

$$L_{\text{diffuse}} = (1 - m) \cdot a \int_{\Omega} L(\omega_i) \frac{\omega_i \cdot n}{\pi} d\omega_i \quad (1)$$

$$L_{\text{specular}} \approx \underbrace{\int_{\Omega} \frac{DFG}{4(\omega_o \cdot n)} \omega_i d\omega_i}_{\text{precomp. BRDF LUT}} \cdot \underbrace{\int_{\Omega} D L(\omega_i) d\omega_i}_{\text{prefiltered Env. Map}}, \quad (2)$$

where $L(\omega_i)$ is the direct incident lighting stored as a 128×128 environment cubemap, n the surface normal. D the GGX microfacet distribution, F Fresnel term, and G

geometric shadowing term.

Optimization. The goal of IR is to optimize shape \mathcal{G} , material reflectance \mathcal{M} , and lighting L of the scene to minimize a re-rendering loss with respect to the input images. Similarly to prior work, we solve the optimization in two stages: (1) optimize for shape \mathcal{G} , followed by (2) a joint estimation of material parameters \mathcal{M} and lighting L . To improve robustness of the two-stage pipeline under sparse input views, we augment each stage with appropriate additional loss terms. We improve geometry estimation (Sec. 4) by leveraging additional learning-based priors from a latent diffusion model and a monocular depth and normal estimation model following established best practices from recent sparse-view Gaussian-based geometry reconstruction methods [8, 34, 35]. We stabilize material and lighting estimation using three complementary learning-based priors: segmentation (Sec. 5.1), IID (Intrinsic Image Decomposition; Sec. 5.2), and diffusion priors (Sec. 5.3).

4. GAINS Stage I: Shape Estimation

We start with the standard 2DGS shape estimation loss, originally formulated for dense input views:

$$\mathcal{L} = \mathcal{L}_{\text{color}} + \lambda_{DD}\mathcal{L}_{DD} + \lambda_{NC}\mathcal{L}_{NC}, \quad (3)$$

where, $\mathcal{L}_{\text{color}} = (1 - \lambda)\mathcal{L}_1 + \lambda\mathcal{L}_{\text{D-SSIM}}$ is a re-rendering loss; \mathcal{L}_{DD} is an optional depth distortion loss, reducing depth ambiguity by bringing intersected Gaussians closer along each ray, and $\mathcal{L}_{NC} = 1 - N_i^T \tilde{N}_i$ is the normal consistency loss with \tilde{N}_i being surface normals obtained from depth.

When applied to sparse input views, the above loss tends to overfit to the captured viewpoints, resulting in significant novel viewpoint artifacts. To better guide the IR optimization towards a robust and generalizable solution, we introduce additional learning based priors: (1) depth and normal guidance, and (2) diffusion guidance.

Depth and Normal Guidance Inspired by prior work [8, 34, 35, 45] that leverages additional depth supervision to alleviate geometric overfitting, we also include a depth loss by enforcing similarity to a monocularly estimated depth \hat{D}_i [12]: $\mathcal{L}_{DC} = 1 - PCC(D_i, \hat{D}_i)$, where $PCC(\cdot)$ is the Pearson Correlation Coefficient. Additionally, we also add a local depth ranking loss \mathcal{L}_{DR} [8] to prevent geometric collapse from hard constraints and alleviate long-range ambiguity. Moreover, given the importance of accurate surface normals in material estimation, we impose normal smoothness via an additional total variation loss $\mathcal{L}_{NS} = TV(N_i, \tilde{N}_i)$, with the reference normals \tilde{N}_i obtained from a monocular depth estimator [12].

Diffusion Guidance Inspired by recent successes in leveraging diffusion models for zero-shot 3D reconstruction [17, 37], we guide the shape reconstruction through Score Distillation Sampling (SDS) towards realistic reconstructions at unseen viewpoints C_j . Concretely, We sample 100 novel

viewpoints for which we render and perform a forward diffusion, yielding noisy latents: $Z_j = \alpha_t \mathcal{R}_{geo}(C_j, \mathcal{G}) + \sigma_t \epsilon$, where timestep $t \sim \mathcal{U}(0.02, 0.98)$ and noise $\epsilon \sim \mathcal{N}(\mathbf{0}, I_0)$. The SDS loss is then calculated as: $\mathcal{L}_{SDS} = \mathbb{E}_{t, \epsilon} [w(t) \|(\epsilon_\phi(Z_j; t) - \epsilon)\|_2^2]$. However, the SDS loss is not effective during early stages of the optimization when the shape reconstruction is far from the target shape. We therefore only include the SDS loss after iteration 10000 (out of 16000).

Summary The total loss function for shape estimation in Stage I is:

$$\mathcal{L}_{geo} = \mathcal{L}_{\text{color}} + \lambda_{DC}\mathcal{L}_{DC} + \lambda_{DR}\mathcal{L}_{DR} + \lambda_{NC}\mathcal{L}_{NC} + \lambda_{NS}\mathcal{L}_{NS} + \lambda_{SDS}\mathcal{L}_{SDS} + \lambda_{BCE}\mathcal{L}_{BCE}, \quad (4)$$

with $\lambda_{DC} = 0.005$, $\lambda_{DR} = 10$, $\lambda_{NC} = 1$, $\lambda_{NS} = 0.005$, $\lambda_{SDS} = 0.0001$. \mathcal{L}_{BCE} denotes an alpha mask rendering loss using a Binary-Cross Entropy (BCE) between the rendered alpha from the learned opacity and ground-truth alpha masks for our sparse inputs. If no ground-truth alpha mask is provided, we assume the scene to reconstruct the background as well, otherwise we set $\lambda_{BCE} = 0.1$. The complete Stage I pipeline is summarized in Fig. 2 (left).

5. GAINS Stage II: Material Properties

In the second stage, we jointly optimize material properties $\mathcal{M} = \{(a_j, r_j, m_j)\}$ and environment lighting L using the re-rendering loss $\mathcal{L}_{\text{color}}$ over 7000 additional iterations. However, multiple combinations of different \mathcal{M} and L produce similar appearances, leading to an ill-posed and ambiguous material estimation. This problem is further exacerbated when only a sparse set of input views is available. Although rendering under the recovered lighting and material properties appears visually plausible, the material properties are overfitted, noisy, inconsistent, and not suitable for relighting (Fig. 1). To alleviate the impact of overfitting under sparse inputs, we complement the loss with additional learning based priors to better guide the optimization towards more plausible material properties, and thus resulting in more robust relighting. We synergize three complementary priors: segmentation (Sec. 5.1), Intrinsic Image Decomposition (IID) (Sec. 5.2), and diffusion guidance (Sec. 5.3).

5.1. Segmentation Guidance

While diffuse albedo varies significantly due to texture variations, we observe that specular material properties are typically consistent within semantically similar regions of an object or scene. This suggests that segmentation cues can help guide the estimation of specular material properties. As a single semantic object can contain multiple subparts with distinct materials, we employ subpart segmentation to define a consistency loss. Instead of constraining the material parameters to be identical for each subpart, we min-

Methods	Synthetic4Relight [44] dataset (8 views)									
	NVS			Albedo			Relight			Roughness
	PSNR \uparrow	SSIM \uparrow	LPIPS \downarrow	PSNR \uparrow	SSIM \uparrow	LPIPS \downarrow	PSNR \uparrow	SSIM \uparrow	LPIPS \downarrow	MSE \downarrow
Ref-GS [36]	24.051	0.832	0.112	17.378	0.832	0.173	24.296	0.858	0.132	0.037
GI-GS [3]	27.047	0.902	0.115	20.479	0.882	0.125	23.923	0.828	0.112	0.056
Ours	30.23	0.943	0.083	22.97	0.914	0.107	25.582	0.916	0.097	0.026

Table 1. **Quantitative evaluation on the synthetic Synthetic4Relight [44] dataset.** Our method estimates better albedo and roughness than baselines leading to better relighting performance. Additionally our method outperforms existing methods in novel-view synthesis. (Red = best, Orange = 2nd best, and Yellow = 3rd best)

Methods	TensorIR [10] dataset (8 views)									Ref-Real [29] dataset (8 views)		
	NVS			Albedo			Relight			NVS		
	PSNR \uparrow	SSIM \uparrow	LPIPS \downarrow	PSNR \uparrow	SSIM \uparrow	LPIPS \downarrow	PSNR \uparrow	SSIM \uparrow	LPIPS \downarrow	PSNR \uparrow	SSIM \uparrow	LPIPS \downarrow
Ref-GS [36]	24.867	0.839	0.119	19.864	0.709	0.219	25.203	0.719	0.129	20.15	0.47	0.353
GI-GS [3]	28.011	0.896	0.111	28.969	0.901	0.121	25.404	0.853	0.135	19.91	0.45	0.371
Ours	29.146	0.915	0.099	27.913	0.912	0.118	26.923	0.892	0.115	21.37	0.56	0.34

Table 2. **Quantitative evaluation on TensorIR [10] dataset and real Ref-Real [29] dataset.** On TensorIR dataset, our method estimates better albedo than existing approaches along with superior relighting results. On Ref-real and TensorIR dataset, our method also performs better novel-view synthesis compared to existing approaches. (Red = best, Orange = 2nd best, and Yellow = 3rd best)

Method Variant	NVS			Albedo			Relight		
	PSNR \uparrow	SSIM \uparrow	LPIPS \downarrow	PSNR \uparrow	SSIM \uparrow	LPIPS \downarrow	PSNR \uparrow	SSIM \uparrow	LPIPS \downarrow
Ours (full)	25.106	0.789	0.236	23.991	0.788	0.276	22.926	0.739	0.274
Ours w/o MI-SDS	25.098	0.788	0.236	24.022	0.788	0.276	22.889	0.737	0.274
Ours w/o Seg	24.862	0.786	0.237	24.214	0.79	0.276	22.894	0.739	0.271
Ours w/o IID	25.148	0.791	0.233	23.706	0.786	0.274	22.878	0.737	0.272
Ours w/o Seg, IID, MI-SDS	24.936	0.788	0.234	23.813	0.785	0.276	22.76	0.738	0.27

Table 3. **Evaluation of the contribution of each learning-based prior used in Stage II of our framework (IID, segmentation (Seg), and diffusion (MI-SDS)) on the tensorIR [10] dataset using 8 viewpoints with best-crop masking.** Removing the IID prior reduces albedo reconstruction fidelity and leads to inconsistent material separation, resulting in degraded relighting performance. Excluding the segmentation prior produces incorrect object and material boundaries, yielding noisy or unstable specular components and harming novel-view synthesis. Finally, removing the diffusion prior leads to an overall drop in performance across all tasks, demonstrating its critical role in stabilizing optimization and improving generalization under sparse-view settings. Overall, the full model consistently achieves the strongest results across NVS, albedo, and relighting, and ablating any component leads to clear and measurable performance degradation. (Red = best, Orange = 2nd best, Yellow = 3rd best)

imize their variance to support mixed materials and to account for imperfect segmentation boundaries.

To include segmentation guidance, we extend the Gaussian primitives with a one-hot vector $E_j = \{0, 1\}^K$ that encodes each Gaussian’s class membership. We employ training-free segmentation mask lifting [2] by rendering SH colored images from V sampled novel view points orbiting the scenery. For each image $\{\hat{f}_v\}_{v=1}^V$ we generate (potentially view-inconsistent) segmentation masks with SAM [22] along with mask-related features $\{f_{v,s} = [g_{v,s}, h_{v,s}]\}_{v=1}^V$ where $f_{v,s}$ is the feature vector for a mask region s of view v and $g_{v,s}, h_{v,s}$ are CLIP [21] and DI-NOv2 [20] features respectively. For each view, we lift the associated mask and features to the Gaussian that contributes most (α -blending wise) and merge already collected Gaussian objects from previous lifting operations with geometric and feature similarity scores.

Next, we leverage the possibly imprecise segmentation masks to define an intra-class consistency (ICC) on the specular roughness and metallicity parameters:

$$\mathcal{L}_{ICC} = \frac{1}{|S_i|} \sum_{s_i \in S_i} \gamma(|s_i|) \cdot (\mathcal{L}_{r,m} + \mathcal{L}_a + \mathcal{L}_e) \quad (5)$$

$$\mathcal{L}_{r,m} = Var(R_{s_i}) + Var(M_{s_i}) \quad (6)$$

$$\mathcal{L}_a = ((1 - R_{s_i}) + M_{s_i}) \cdot \frac{1}{3} \sum_{c=1}^3 Var(A_{s_i}^{(c)}) \quad (7)$$

$$\mathcal{L}_e = ((1 - M_{s_i}) + R_{s_i}) \cdot E_{s_i} \quad (8)$$

where S_i is the set of all masks rendered from a captured viewpoint i , A_{s_i} , R_{s_i} , and M_{s_i} are the rendered masked albedo, roughness, and metallicity, along with E_{s_i} representing the masked re-render loss. $\gamma(|s_i|) = \exp(25 \cdot \frac{|I_i||s_i|}{|S_i|^2})$ is a scaling function depending on the size of the

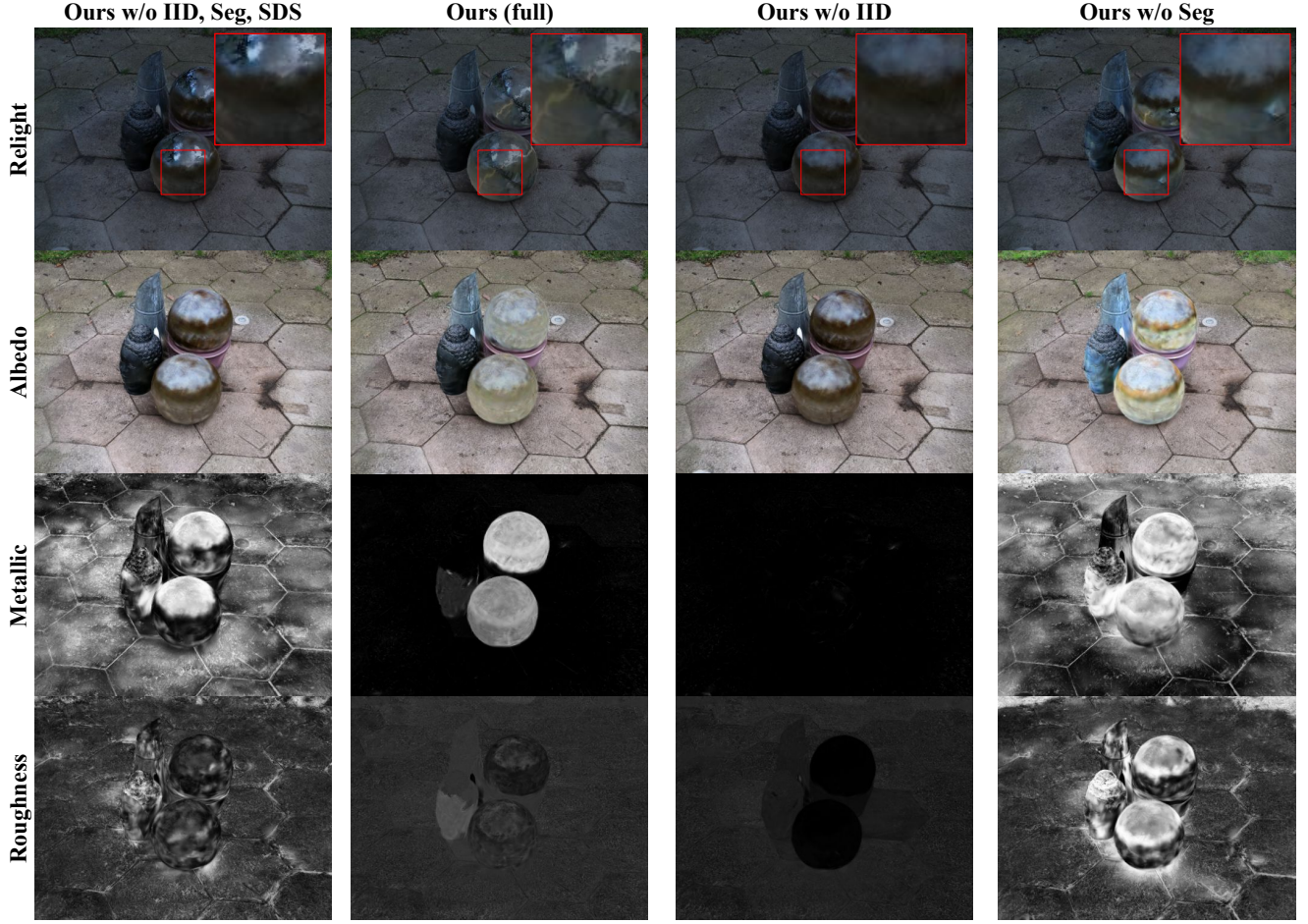


Figure 3. **Ablation studies on the *gardensphere* scene from the Ref-Real [29] dataset.** In absence of learning-based priors (Ours w/o IID, Seg, SDS in 1st col) reflectance maps are poorly reconstructed, especially metallicity and roughness. Without the IID prior (3rd col) results in weaker specular effects (compared to the 2nd col). Without segmentation guidance (4th col) results in noise material maps across objects.

mask s_i . The first variance reduction term $\mathcal{L}_{r,m}$ reduces irregularities for specular roughness and metallic across all masks. While in general we attribute texture variations to the diffuse texture, an ambiguity exists in the case of mirror-like materials that reflects texture from the environment lighting. To address this ambiguity, we bias the optimization to attribute texture details to specular reflections in the case of mirror-like materials by adding a loss term \mathcal{L}_a that encourages a variance reduction in diffuse albedo in regions where we observe low roughness and high metallicity. Lastly, regions with high specularity typically suffer from larger geometry errors, and thus higher material estimation errors. We therefore, include a loss term that prefers higher specularity in regions with large reconstruction errors.

5.2. Intrinsic Image Decomposition Prior

While segmentation improves consistency in roughness and metallicity over multiple viewpoints, it is not suited for

diffuse albedo which often contains high-frequency texture variations that are difficult to estimate from sparse viewpoints. In the absence of appropriate regularization, the model will overfit diffuse albedo and fail to disentangle lighting effects from intrinsic albedo, which ultimately leads to a subpar relighting performance.

Recent advances in monocular Intrinsic Image Decomposition (IID) [12, 40] enable high quality diffuse albedo decompositions, albeit potentially view-inconsistent. We therefore propose to leverage the IID to regularize the diffuse albedo estimation while accounting for potential view-inconsistencies:

$$\mathcal{L}_{IID} = \beta(\tau) \cdot \mathcal{L}_2(A_i, \hat{A}_i), \quad (9)$$

where \hat{A}_i is the IID diffuse albedo for the captured image I_i obtained using RGB-X [40]. To mitigate the influence of view-inconsistency in the IID, we weight the loss by $\beta(\tau)$ (a linear decrease) which depends on the current iteration step τ , thereby relaxing the influence of the IID diffuse

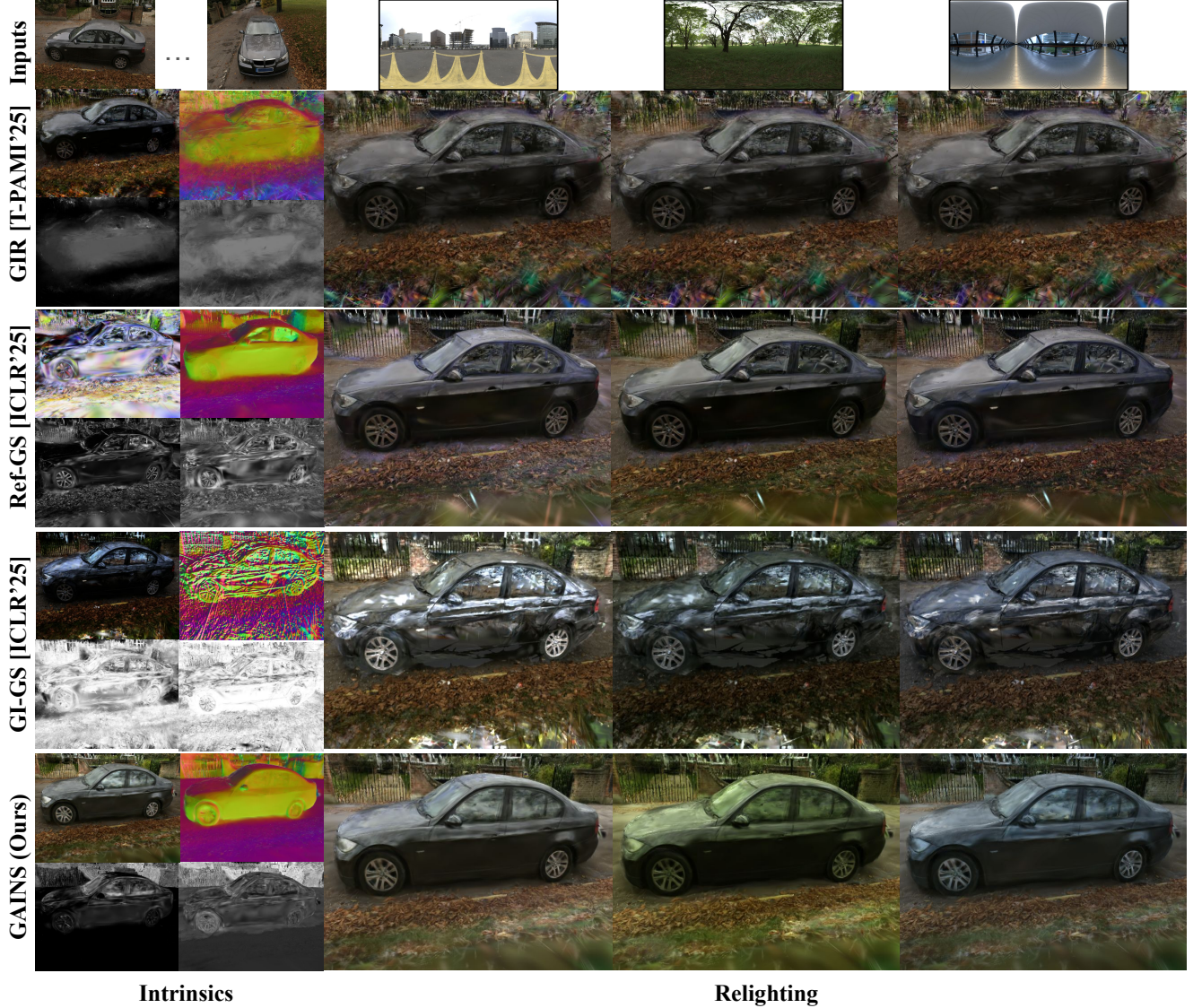


Figure 4. **Qualitative comparison of intrinsic estimation and relighting on the *sedan* scene from the Ref-Real dataset [29] reconstructed from 8 views.** Column 1 shows novel-view intrinsic renderings in a 2×2 layout: (top) rendered albedo and surface normals, (bottom) specular roughness and metallicity. Columns 2–4 show relighting results under three different environment maps from novel viewpoints. GAINS recovers significantly more accurate intrinsics, enabling more realistic relighting.

albedo as the model converges. We opt against using additional IID supervision for specular roughness and metallicity as we found these parameters to be less robust and exhibit more inconsistencies across views

5.3. Multi-illuminated Score Distillation Sampling

While both segmentation guidance and IID guidance improve the accuracy of the specular and diffuse material properties respectively, they do not necessarily provide good generalization to novel viewpoints or lighting. To address these issues, we take inspiration from our usage of SDS in the first stage to aid in reducing unrealistic artifacts on novel viewpoints, and introduce a modified SDS loss to

improve view and lighting-consistency for material properties. To avoid overfitting to the learned environment map L , we render relit images $\mathcal{R}_{mat}(C_j, \mathcal{G}, \mathcal{M}, \mathcal{E}_l)$ from a novel view C_j under randomly selected lighting from a predetermined set $\{\mathcal{E}_l\}_{l=1}^{|\mathcal{E}|}$, and define the SDS loss as:

$$\mathcal{L}_{MI-SDS} = \mathbb{E}_{t, \epsilon} \left[w(t) \| (\epsilon_\phi(Z_j^l; t) - \epsilon) \|_2^2 \right], \quad (10)$$

where $Z_j^l = \alpha_t \mathcal{R}_{mat}(C_j, \mathcal{G}, \mathcal{M}, \mathcal{E}_l) + \sigma_t \epsilon$ is the noisy diffusion latent of the rendered scene under novel view and lighting. Similarly as in the geometry reconstruction stage, we start the diffusion guidance once the optimization solution has stabilized (*i.e.*, after 3000 steps).

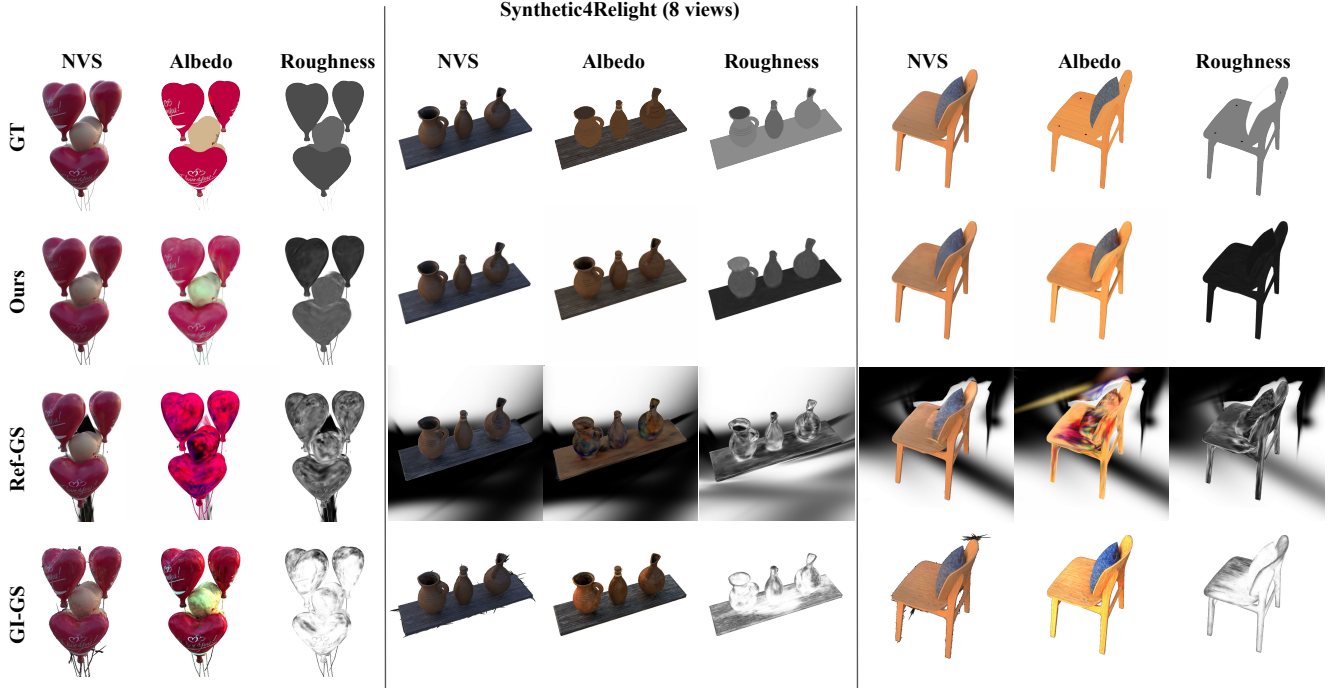


Figure 5. **Qualitative comparison of albedo and roughness estimation and novel-view synthesis (NVS) on Synthetic4Relight [44] dataset trained with 8 views.** While all methods produce reasonable NVS, our method’s estimates significantly better albedo and roughness than GI-GS and Ref-GS that overfit to limited training views and fail to disentangle reflectance from lighting.

5.4. Final Loss

Each loss contributes to a specific enhancement of the material estimation process: parameter accuracy, multi-view consistency, or novel views and lighting generalization. We combine all losses as:

$$\mathcal{L}_{mat} = \mathcal{L}_{color} + \lambda_{ICC}\mathcal{L}_{ICC} + \lambda_{IID}\mathcal{L}_{IID} + \lambda_{MI-SDS}\mathcal{L}_{MI-SDS} + \lambda_{TV}\mathcal{L}_{TV},$$

where $\lambda_{ICC} = 0.1$, $\lambda_{IID} = 1$, $\lambda_{MI-SDS} = 0.0001$ and $\lambda_{TV} = 1$. \mathcal{L}_{TV} represents a total variation loss on our reconstructed lighting, acting as a smoothing term. Fig. 2 (right) summarizes the full Stage II pipeline.

6. Evaluation

Evaluation Framework. We compare GAINS against state-of-the-art IR frameworks that use Gaussian Splatting for both objects and scenes: Ref-GS [36] and GI-GS [3] over two synthetic datasets (TensorIR [10] for NVS, albedo and relighting; and Synthetic4Relight [44] for NVS, albedo, relighting and roughness), and a real-world dataset (Ref-Real [29]), on which we quantitatively evaluate NVS performance only. We also evaluated GIR [26] on real scenes from Ref-Real, but we found that it fails to reconstruct meaningful geometry and reflectance (Fig. 4) while requiring long per-scene training time (over 7 hours). Therefore, we opted not to include GIR in the evaluation over the

synthetic datasets. We evaluate NVS, albedo, and relighting using three metrics: PSNR, SSIM and LPIPS, while for roughness we employ MSE. We employ scale invariant losses to evaluate albedo of all approaches by uniformly scaling each albedo map to minimize MSE w.r.t. ground-truth before applying an error metric. Unless specified otherwise, all evaluations are performed with 8 sparse views uniformly sampled from the dense views.

Performance Evaluation. Tab. 1, and 2 quantitatively summarize the comparison for the three datasets. In general, GAINS yields more accurate albedo maps and relighting across both TensorIR and Synthetic4Relight compared to all prior methods. Additionally, we demonstrate that our roughness estimations also surpass current methods. Furthermore, GAINS achieves overall better results for NVS than all competing methods. However, error metrics do not always capture important visual differences. Therefore, we also provide qualitative comparisons in Fig. 1, 4, and 5. From the qualitative comparison, especially on the real-world Ref-Real dataset (Fig. 1 and 4), we note less baking of specular reflections, and generally more accurate relighting results, *e.g.*, the reflections of the ground (missing for Ref-GS) and the sky (baking of captured reflection for both Ref-GS and GI-GS) on the ball in Fig. 1. Furthermore, while GI-GS almost slightly competes in NVS against our method, we observe that it produces less accurate shape and

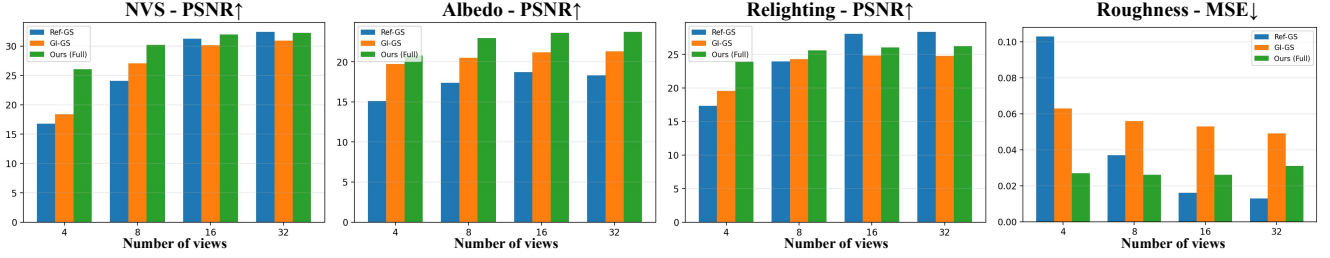


Figure 6. **Comparison of our method with Ref-GS [36] and GI-GS [3] on the Synthetic4Relight [44] dataset for an increasing numbers of input views.** The figure is organized into: PSNR for novel-view synthesis (top left), albedo (top right), and relighting (bottom left), and MSE for roughness (bottom right). Each bar chart shows results for 4, 8, 16, and 32 input views, with blue indicating Ref-GS, orange indicating GI-GS, and green indicating GAINS (ours). GAINS consistently surpasses both baselines in sparse-view settings (4-8 views) and remains competitive as the number of views increases.

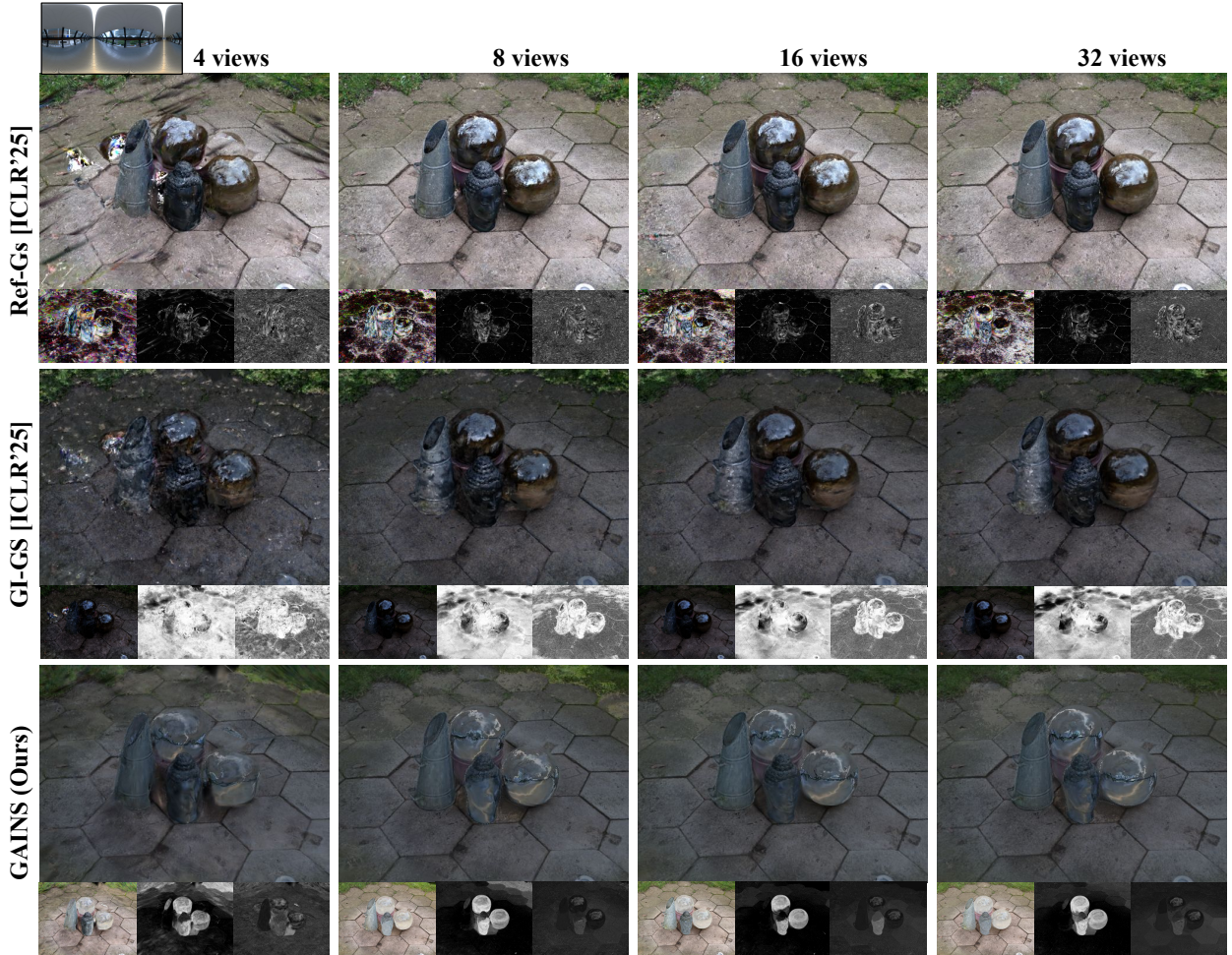


Figure 7. **Relighting and material estimation comparison for varying number of views on the gardenspheres scene from the Ref-Real [29] dataset.** We visualize for each method (rows: Ref-GS [36], GI-GS [3], and GAINS (ours)) relit results for 4, 8, 16, and 32 input views. For each result, we show the relit result under the *bridge* environment map, as well as (from left to right) the estimated albedo, metallic, and roughness. GAINS consistently produces robust relighting and material estimations even from sparse views. In contrast competing methods struggle to recover accurate materials, yielding degraded relighting quality.

normals (e.g., the noisy normals on the car in the sedan scene in Fig. 4), indicating that the GI-GS NVS performance is mainly due to overfitting. As shown in Fig. 5, our method demonstrates a clear advantage in material estimation under sparse-view settings. While Ref-GS suffers from floaters and GI-GS typically recovers reasonable geometry but fails to produce accurate or stable albedo and roughness maps, our approach, supported by learning-based priors, delivers consistently superior NVS quality as well as more reliable albedo and roughness estimations across all scenes.

View-dependent Performance. In addition to our comprehensive quantitative and qualitative evaluation on both synthetic and real datasets, we further analyze the behavior of our method as the number of available input views increases. Fig. 6 summarizes the quantitative comparison for PSNR on NVS, albedo, relighting, and roughness on the Synthetic4Relight [44] dataset. We observe that in sparse-view scenarios (4-8 views), our method consistently outperforms all baselines across all evaluation scenarios. As the number of views increases (16-32), Ref-GS in particular achieves better performance in NVS and relighting; however, our method continues to produce competitive results within a small margin. Notably, while all methods benefit from additional views, GAINS starts from a more stable and reliable baseline in the extremely sparse-view regime, indicating stronger robustness under challenging conditions. A closer inspection of the roughness estimation reveals that our method maintains stable and consistent roughness predictions regardless of view count due to segmentation guidance. In contrast, techniques such as Ref-GS, which impose no spatial constraints, eventually surpass our performance at higher view counts by capturing finer-grained roughness estimations that segmentation-based guidance is unable to capture. This illustrates a minor trade-off between robustness in sparse-view settings and the potential for high-frequency detail recovery under dense supervision. Complementing our quantitative experiments, we also provide qualitative relighting and material estimation results (albedo, metallicity, and roughness) in Fig. 7 on the *garden-spheres* scene from the Ref-Real [29] dataset. Across all view counts, GAINS demonstrates strong and stable material reconstruction, producing accurate specular reflections and consequently superior relighting performance. As reflected quantitatively in the roughness bar chart, this trend is also clearly visible in the qualitative results. Specifically, our roughness and metallic estimates remain stable and robust, exhibiting only minor improvements as the number of input views increases. This further demonstrates GAINS’ advantage in low-view settings, where competing methods often suffer from noisy, irregular, or unstable material reconstructions. Improvements observed under dense inputs mainly stem from enhanced geometry estimation and improved lighting recovery. In contrast competing methods

exhibit pronounced shape degradation in low-view settings (4-8 views).

Ablation. We conduct an ablation study on the TensoIR [10] dataset using 8 input views with a best-crop masking strategy to ensure that metrics reflect only the reconstructed foreground regions. We focus our ablation on the different learning-based priors that constitute the material estimation stage (II): segmentation guidance, IID guidance, and the diffusion prior. In addition, we also include a comparison to baseline that includes only the additional losses for shape, but not for material estimation. From Tab. 3, we observe that the IID component improves the accuracy of the albedo estimation and relighting quality, but compared to segmentation guidance or the diffusion prior, NVS quality degrades. Segmentation guidance improves NVS performance. The diffusion prior by itself improves all components, albeit to a lesser degree than IID for albedo and relighting. However, when combining all three components, we see the overall best performance. Fig. 3 provides further qualitative evidence of these effects. Here we demonstrate how in the absence of learning-based priors, our method fails to recover reliable reflectance properties, with metallicity and roughness being especially inaccurate. When the IID prior is omitted, specular responses become significantly diminished, while removing segmentation guidance prevents the model from learning consistent material assignments across object regions.

7. Conclusion

We introduced GAINS, a Gaussian-based inverse rendering framework tailored for sparse-view settings. By combining segmentation, IID, and diffusion priors within a two-stage optimization pipeline, GAINS effectively stabilizes geometry and material estimation. Extensive experiments on synthetic and real-world datasets show that GAINS achieves state-of-the-art relighting accuracy and competitive novel-view synthesis compared to prior Gaussian-based IR methods. Qualitative results further demonstrate improved material-lighting separation and reduced reflection baking. GAINS highlights the power of synergizing complementary learning priors for physically consistent inverse rendering under sparse observations.

Acknowledgments: This work is partially supported by a National Institute of Health (NIH) NIBIB project #R21EB035832 and #R21EB037440. Patrick Noras is supported by the DAAD-PROMOS scholarship during their research stay as a visiting scholar at the University of North Carolina at Chapel Hill.

References

- [1] Brent Burley and Walt Disney Animation Studios. Physically-based shading at disney. In *Acm siggraph*, pages 1–7. vol. 2012, 2012. 3
- [2] Rohan Chacko, Nicolai Häni, Eldar Khaliullin, Lin Sun, and Douglas Lee. Lifting by gaussians: A simple, fast and flexible method for 3d instance segmentation. In *2025 IEEE/CVF Winter Conference on Applications of Computer Vision (WACV)*, pages 3497–3507. IEEE, 2025. 5
- [3] Hongze Chen, Zehong Lin, and Jun Zhang. Gi-gs: Global illumination decomposition on gaussian splatting for inverse rendering. In *ICLR*, 2025. 1, 2, 3, 5, 8, 9, 7, 10, 11
- [4] Paul Debevec, Chris Tchou, Andrew Gardner, Tim Hawkins, Charis Poullis, Jessi Stumpfel, Andrew Jones, Nathaniel Yun, Per Einarsson, Therese Lundgren, et al. Estimating surface reflectance properties of a complex scene under captured natural illumination. 2004. 2
- [5] Chun Gu, Xiaofei Wei, Zixuan Zeng, Yuxuan Yao, and Li Zhang. IRGS: Inter-Reflective Gaussian Splatting with 2D Gaussian Ray Tracing, 2025. 2
- [6] Jon Hasselgren, Nikolai Hofmann, and Jacob Munkberg. Shape, Light, and Material Decomposition from Images using Monte Carlo Rendering and Denoising. 2
- [7] Binbin Huang, Zehao Yu, Anpei Chen, Andreas Geiger, and Shenghua Gao. 2d gaussian splatting for geometrically accurate radiance fields. In *SIGGRAPH 2024 Conference Papers*. Association for Computing Machinery, 2024. 3
- [8] Han Huang, Yulun Wu, Chao Deng, Ge Gao, Ming Gu, and Yu-Shen Liu. Fatesgs: Fast and accurate sparse-view surface reconstruction using gaussian splatting with depth-feature consistency. In *Proceedings of the AAAI Conference on Artificial Intelligence*, 2025. 2, 3, 4
- [9] Yingwenqi Jiang, Jiadong Tu, Yuan Liu, Xifeng Gao, Xiaoxiao Long, Wenping Wang, and Yuexin Ma. Gaussianshader: 3d gaussian splatting with shading functions for reflective surfaces. *arXiv preprint arXiv:2311.17977*, 2023. 2
- [10] Haian Jin, Isabella Liu, Peijia Xu, Xiaoshuai Zhang, Songfang Han, Sai Bi, Xiaowei Zhou, Zexiang Xu, and Hao Su. Tensoir: Tensorial inverse rendering. In *Proceedings of the IEEE/CVF Conference on Computer Vision and Pattern Recognition (CVPR)*, 2023. 2, 5, 8, 10, 1, 3, 7, 9, 11
- [11] Brian Karis and Epic Games. Real shading in unreal engine 4. *Proc. Physically Based Shading Theory Practice*, 4(3):1, 2013. 3
- [12] Bingxin Ke, Anton Obukhov, Shengyu Huang, Nando Metzger, Rodrigo Caye Daudt, and Konrad Schindler. Repurposing diffusion-based image generators for monocular depth estimation. In *Proceedings of the IEEE/CVF Conference on Computer Vision and Pattern Recognition (CVPR)*, 2024. 4, 6
- [13] Bernhard Kerbl, Georgios Kopanas, Thomas Leimkühler, and George Drettakis. 3d gaussian splatting for real-time radiance field rendering. *ACM Transactions on Graphics*, 42(4), 2023. 2, 3
- [14] Zhengqin Li, Mohammad Shafiei, Ravi Ramamoorthi, Kalyan Sunkavalli, and Manmohan Chandraker. Inverse Rendering for Complex Indoor Scenes: Shape, Spatially-Varying Lighting and SVBRDF From a Single Image. In *2020 IEEE/CVF Conference on Computer Vision and Pattern Recognition (CVPR)*, pages 2472–2481, Seattle, WA, USA, 2020. IEEE. 2, 3
- [15] Zhihao Liang, Qi Zhang, Ying Feng, Ying Shan, and Kui Jia. Gs-ir: 3d gaussian splatting for inverse rendering. In *Proceedings of the IEEE/CVF Conference on Computer Vision and Pattern Recognition*, pages 21644–21653, 2024. 2
- [16] Daniel Lichy, Jiaye Wu, Soumyadip Sengupta, and David W Jacobs. Shape and material capture at home. In *Proceedings of the IEEE/CVF Conference on Computer Vision and Pattern Recognition*, pages 6123–6133, 2021. 2
- [17] Ruoshi Liu, Rundi Wu, Basile Van Hoorick, Pavel Tokmakov, Sergey Zakharov, and Carl Vondrick. Zero-1-to-3: Zero-shot one image to 3d object, 2023. 4
- [18] Yuan Liu, Peng Wang, Cheng Lin, Xiaoxiao Long, Jiepeng Wang, Lingjie Liu, Taku Komura, and Wenping Wang. NeRO: Neural Geometry and BRDF Reconstruction of Reflective Objects from Multiview Images. *ACM Trans. Graph.*, 42(4):114:1–114:22, 2023. 2
- [19] Ben Mildenhall, Pratul P. Srinivasan, Matthew Tancik, Jonathan T. Barron, Ravi Ramamoorthi, and Ren Ng. Nerf: Representing scenes as neural radiance fields for view synthesis, 2020. 2
- [20] Maxime Oquab, Timothée Darcet, Theo Moutakanni, Huy V. Vo, Marc Szafraniec, Vasil Khalidov, Pierre Fernandez, Daniel Haziza, Francisco Massa, Alaaeldin El-Nouby, Russell Howes, Po-Yao Huang, Hu Xu, Vasu Sharma, Shang-Wen Li, Wojciech Galuba, Mike Rabbat, Mido Assran, Nicolas Ballas, Gabriel Synnaeve, Ishan Misra, Herve Jegou, Julien Mairal, Patrick Labatut, Armand Joulin, and Piotr Bojanowski. Dinov2: Learning robust visual features without supervision, 2023. 5
- [21] Alec Radford, Jong Wook Kim, Chris Hallacy, Aditya Ramesh, Gabriel Goh, Sandhini Agarwal, Girish Sastry, Amanda Askell, Pamela Mishkin, Jack Clark, et al. Learning transferable visual models from natural language supervision. In *International conference on machine learning*, pages 8748–8763. PmLR, 2021. 5
- [22] Nikhila Ravi, Valentin Gabeur, Yuan-Ting Hu, Ronghang Hu, Chaitanya Ryali, Tengyu Ma, Haitham Khedr, Roman Rädle, Chloe Rolland, Laura Gustafson, Eric Mintun, Junting Pan, Kalyan Vasudev Alwala, Nicolas Carion, Chao-Yuan Wu, Ross Girshick, Piotr Dollár, and Christoph Feichtenhofer. Sam 2: Segment anything in images and videos. *arXiv preprint arXiv:2408.00714*, 2024. 5
- [23] Yoichi Sato, Mark D Wheeler, and Katsushi Ikeuchi. Object shape and reflectance modeling from observation. In *Proceedings of the 24th annual conference on Computer graphics and interactive techniques*, pages 379–387, 1997. 2
- [24] Soumyadip Sengupta, Angjoo Kanazawa, Carlos D. Castillo, and David W. Jacobs. SfSNet: Learning Shape, Reflectance and Illuminance of Faces ‘in the Wild’. In *Proceedings of the IEEE Conference on Computer Vision and Pattern Recognition*, pages 6296–6305, 2018. 2, 3
- [25] Soumyadip Sengupta, Jinwei Gu, Kihwan Kim, Guilin Liu, David W Jacobs, and Jan Kautz. Neural inverse rendering

- of an indoor scene from a single image. In *Proceedings of the IEEE/CVF International Conference on Computer Vision*, pages 8598–8607, 2019. 2, 3
- [26] Yahao Shi, Yanmin Wu, Chenming Wu, Xing Liu, Chen Zhao, Haocheng Feng, Jian Zhang, Bin Zhou, Errui Ding, and Jingdong Wang. Gir: 3d gaussian inverse rendering for relightable scene factorization. *IEEE Transactions on Transactions on Pattern Analysis and Machine Intelligence*, 2025. 2, 3, 8, 1, 5
- [27] Pratul P Srinivasan, Boyang Deng, Xiuming Zhang, Matthew Tancik, Ben Mildenhall, and Jonathan T Barron. Nerv: Neural reflectance and visibility fields for relighting and view synthesis. In *Proceedings of the IEEE/CVF conference on computer vision and pattern recognition*, pages 7495–7504, 2021. 2
- [28] Cheng Sun, Guangyan Cai, Zhengqin Li, Kai Yan, Cheng Zhang, Carl Marshall, Jia-Bin Huang, Shuang Zhao, and Zhao Dong. Neural-PBIR Reconstruction of Shape, Material, and Illumination. In *2023 IEEE/CVF International Conference on Computer Vision (ICCV)*, pages 18000–18010, Paris, France, 2023. IEEE. 2
- [29] Dor Verbin, Peter Hedman, Ben Mildenhall, Todd Zickler, Jonathan T. Barron, and Pratul P. Srinivasan. Ref-NeRF: Structured view-dependent appearance for neural radiance fields. *CVPR*, 2022. 2, 5, 6, 7, 8, 9, 10, 1
- [30] Guangcong Wang, Zhaoxi Chen, Chen Change Loy, and Ziwei Liu. Sparsenerf: Distilling depth ranking for few-shot novel view synthesis. In *Proceedings of the IEEE/CVF international conference on computer vision*, pages 9065–9076, 2023. 3
- [31] Haoyuan Wang, Wenbo Hu, Lei Zhu, and Rynson W.H. Lau. Inverse Rendering of Glossy Objects via the Neural Plenoptic Function and Radiance Fields. In *2024 IEEE/CVF Conference on Computer Vision and Pattern Recognition (CVPR)*, pages 19999–20008, Seattle, WA, USA, 2024. IEEE. 2
- [32] Jiaye Wu, Saeed Hadadan, Geng Lin, Matthias Zwicker, David Jacobs, and Roni Sengupta. Gani: Global and near field illumination aware neural inverse rendering. *arXiv preprint arXiv:2403.15651*, 2024. 2
- [33] Rui Xia, Yue Dong, Pieter Peers, and Xin Tong. Recovering shape and spatially-varying surface reflectance under unknown illumination. *ACM Transactions on Graphics (ToG)*, 35(6):1–12, 2016. 2
- [34] Haolin Xiong, Sairisheek Muttukuru, Rishi Upadhyay, Pradyumna Chari, and Achuta Kadambi. Sparsegs: Real-time 360° sparse view synthesis using gaussian splatting. *Arxiv*, 2023. 2, 3, 4
- [35] Chen Yang, Sikuang Li, Jiemin Fang, Ruofan Liang, Lingxi Xie, Xiaopeng Zhang, Wei Shen, and Qi Tian. Gaussianobject: High-quality 3d object reconstruction from four views with gaussian splatting. *ACM Transactions on Graphics*, 43(6), 2024. 2, 3, 4
- [36] Yuxuan Yao, Zixuan Zeng, Chun Gu, Xiatian Zhu, and Li Zhang. Reflective gaussian splatting. *arXiv preprint*, 2024. 1, 2, 3, 5, 8, 9, 7, 10, 11
- [37] Taoran Yi, Jiemin Fang, Junjie Wang, Guanjun Wu, Lingxi Xie, Xiaopeng Zhang, Wenyu Liu, Qi Tian, and Xinggang Wang. Gaussiandreamer: Fast generation from text to 3d gaussians by bridging 2d and 3d diffusion models. In *CVPR*, 2024. 4
- [38] Ye Yu and William A. P. Smith. Inverserendernet: Learning single image inverse rendering. In *Proceedings of the IEEE/CVF Conference on Computer Vision and Pattern Recognition (CVPR)*, 2019. 2
- [39] Chong Zeng, Guojun Chen, Yue Dong, Pieter Peers, Hongzhi Wu, and Xin Tong. Relighting neural radiance fields with shadow and highlight hints. In *ACM SIGGRAPH 2023 Conference Proceedings*, pages 1–11, 2023. 2
- [40] Zheng Zeng, Valentin Deschaintre, Iliyan Georgiev, Yannick Hold-Geoffroy, Yiwei Hu, Fujun Luan, Ling-Qi Yan, and Miloš Hašan. Rgb \leftrightarrow x: Image decomposition and synthesis using material- and lighting-aware diffusion models, 2024. 6
- [41] Jingyang Zhang, Yao Yao, Shiwei Li, Jingbo Liu, Tian Fang, David McKinnon, Yanghai Tsin, and Long Quan. NeILF++: Inter-Reflectable Light Fields for Geometry and Material Estimation. In *2023 IEEE/CVF International Conference on Computer Vision (ICCV)*, pages 3578–3587, Paris, France, 2023. IEEE. 2
- [42] Tianyuan Zhang, Zhengfei Kuang, Haian Jin, Zexiang Xu, Sai Bi, Hao Tan, He Zhang, Yiwei Hu, Milos Hasan, William T Freeman, et al. Relitlm: Generative relightable radiance for large reconstruction models. *arXiv preprint arXiv:2410.06231*, 2024. 3
- [43] Xiuming Zhang, Pratul P Srinivasan, Boyang Deng, Paul Debevec, William T Freeman, and Jonathan T Barron. Nerfactor: Neural factorization of shape and reflectance under an unknown illumination. *ACM Transactions on Graphics (ToG)*, 40(6):1–18, 2021. 2
- [44] Yuanqing Zhang, Jiaming Sun, Xingyi He, Huan Fu, Rongfei Jia, and Xiaowei Zhou. Modeling indirect illumination for inverse rendering. In *CVPR*, 2022. 2, 5, 8, 9, 10, 1
- [45] Zehao Zhu, Zhiwen Fan, Yifan Jiang, and Zhangyang Wang. Fsgs: Real-time few-shot view synthesis using gaussian splatting, 2023. 3, 4

GAINS: Gaussian-based Inverse Rendering from Sparse Multi-View Captures

Supplementary Material

A. Overview of Appendices

We categorize our appendices in the following way:

- [Sec. B](#) provides additional details of our experimental setup, including the computational resources used and factors influencing the performance of our method.
- [Sec. C](#) presents additional visual results on the TensorIR [10] and Ref-Real [29] datasets, along with intermediate segmentation maps produced during training. We include reconstructions to highlight the stability and robustness of our method.

B. Experiment, and Performance Details

Unless stated otherwise, all experiments were conducted on a single NVIDIA RTX A4500 GPU with 20 GB of VRAM. Our method operates in linear color space; datasets provided in sRGB are internally linearized, and final predictions are converted back to sRGB before computing the corresponding loss terms. This ensures that all color-dependent computations remain physically consistent while metrics remain comparable to prior work.

Training efficiency depends on two factors: the timing of the diffusion-prior activation and the number of views used during the intermediate segmentation-lifting stage. In our default configuration, the average training time per scene is approximately 1.5 hours. Notably, segmentation quality has an impact on the performance of the Gaussian representation. While using more views for the iterative segmentation merging improves consistency and reduces object-level ambiguities, it also increases computational overhead: 1min for 25 views and 5mins for 100 views. This trade-off becomes particularly important in novel-view synthesis (NVS) and relighting tasks, where inaccurate or overly coarse segmentation (e.g., multiple materials merging into a single region or a single region being split up into multiple segmentation classes) can degrade the final reconstruction. This performance decrease is however not severe and thus for all conducted experiments a total of 100 novel render viewpoints are leveraged to create a robust segmentation.

C. Additional Results

We present additional qualitative results to further validate the effectiveness of our method. [Fig. 8](#) and [9](#) provide qualitative comparisons on the TensorIR dataset [10], specifically on the *hotdog* and *lego* scenes. Our method demonstrates stronger robustness and improved fidelity relative to existing Gaussian-based inverse-rendering methods. [Fig. 10](#) shows reconstructed segmentation maps for several representative scenes, highlighting the structural coherence of our lifted segmentation across viewpoints. Following the

demonstration of our segmentation results, we visualize the impact of the number of views used for the segmentation lifting and merging procedure in [Fig. 11](#), highlighting the loss of material accuracy that is coupled to the quality of the recovered segmentation. [Fig. 12](#) includes the *toy car* scene from the Ref-Real [29] dataset and compares our method to current baselines, including Ref-GS [36], GI-GS [3], and GIR [26]. Our method produces more faithful material decomposition and relighting behavior while reducing visual artifacts present in competing approaches. Furthermore, [Fig. 13](#) extends the qualitative comparison on the *toy car* scene by illustrating the impact on material and relighting performance with 4 and 16 views. We observe how our method degrades less in quality when decreasing the number of input views, while current Gaussian-based inverse-rendering techniques demonstrate notable quality reduction. [Fig. 14](#), [15](#), [16](#) and [17](#) extend the prior discussion on relighting performance by providing an extensive qualitative comparison across all scenes of the TensorIR [10] dataset under five different novel lighting conditions. Across all scenes and environment maps, our method consistently produces the most faithful and visually coherent relighting results. Ref-GS is often affected by floaters. Furthermore, Ref-GS also produces visually overly flat and muted relighting outputs. GI-GS, in contrast, struggles with incorrectly reconstructed high-frequency regions, leading to highly inconsistent lighting effects, an issue likely rooted in its weaker normal prediction and less accurate geometry reconstruction. [Fig. 18](#) presents additional bar charts to illustrate the view-dependent performance on the TensorIR [10] dataset. The observed trends closely mirror those seen in our earlier Synthetic4Relight [44] experiments. Specifically, in sparse-view settings (4-8 views), our method surpasses all baselines across nearly all metrics for NVS, albedo, and relighting. As the number of input views increases (16-32), Ref-GS begins to slightly outperform our method in selected metrics, although the margin remains small and our approach continues to compete strongly. Overall, while all methods benefit from additional views, ours demonstrates a clear advantage in extremely sparse-view scenarios by starting from a substantially stronger and more stable baseline.

tensorIR: Hotdog (8 views)					
	NVS	Normal	Albedo	Relight (Fireplace)	Relight (Bridge)
GT					
Ref-GS					
	PSNR: 7.4 SSIM: 0.71 LPIPS: 0.234	MAE: 26.12	PSNR: 2.079 SSIM: 0.19 LPIPS: 0.53	PSNR: 7.94 SSIM: 0.71 LPIPS: 0.29	PSNR: 8.39 SSIM: 0.71 LPIPS: 0.255
GI-GS					
	PSNR: 15.56 SSIM: 0.91 LPIPS: 0.111	MAE: 25.04	PSNR: 22.08 SSIM: 0.87 LPIPS: 0.162	PSNR: 23.13 SSIM: 0.87 LPIPS: 0.15	PSNR: 19.99 SSIM: 0.79 LPIPS: 0.185
Ours					
	PSNR: 27.19 SSIM: 0.93 LPIPS: 0.066	MAE: 17.17	PSNR: 25.18 SSIM: 0.92 LPIPS: 0.066	PSNR: 23.93 SSIM: 0.9 LPIPS: 0.111	PSNR: 22.06 SSIM: 0.87 LPIPS: 0.115

Figure 8. Comparison of our method with Ref-GS [36] and GI-GS [3] on the *hotdog* scene from the TensorIR [10] dataset, reconstructed from 8 input views. From top to bottom, the rows show the ground-truth reference, Ref-GS, GI-GS and GAINS (our method). The columns present, from left to right: NVS renderings, predicted surface normals, albedo reconstruction, and relighting results. To compensate for the albedo-lighting intensity ambiguity, we multiply each method’s relighting results by a global scale factor that minimizes the MSE error with respect to the ground truth. For the *hotdog* scene, relighting is performed under the *fireplace* and *bridge* environment map. Our method yields cleaner geometry with significantly fewer floaters, producing sharper and more coherent surface normals. This improved geometric consistency, coupled with our segmentation-driven material recovery, results in more stable and visually persuasive relighting when compared to Ref-GS and GI-GS. Overall, our approach achieves competitive or improved results across all evaluation axes (NVS, normals, albedo, and relighting), demonstrating the effectiveness of our reconstruction pipeline in low-view settings.

tensorIR: Lego (8 views)

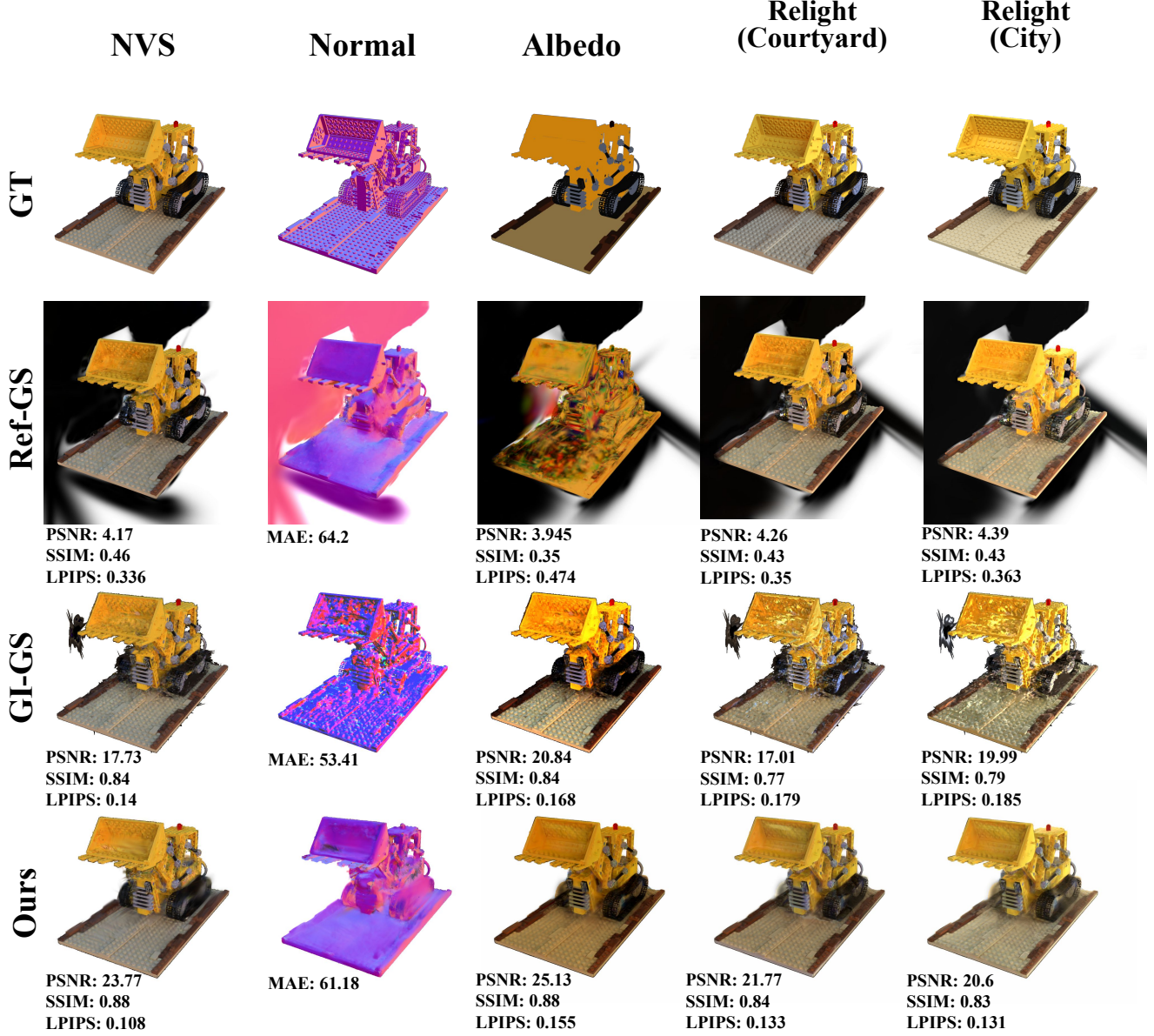


Figure 9. Comparison of our method with Ref-GS [36] and GI-GS [3] on the *lego* scene from the TensorIR [10] dataset, reconstructed from 8 input views. From top to bottom, the rows show the ground-truth reference, Ref-GS, GI-GS and GAINS (our method). The columns present, from left to right: NVS renderings, predicted surface normals, albedo reconstruction, and relighting results. To compensate for the albedo-lighting intensity ambiguity, we multiply each method’s relighting results by a global scale factor that minimizes the MSE error with respect to the ground truth. For the *lego* scene, relighting is shown under the *courtyard* and *city* illumination. Similar to our previous comparison on the *hotdog* scene, our method produces robust geometry with little floaters. In combination with our segmentation-driven material recovery, results are more stable and visually superior in context of relighting when compared to Ref-GS and GI-GS.



Figure 10. **Reconstructed segmentation maps generated by our iterative lifting procedure.** The first row shows the reference ground truth images, while the second row displays our rendered segmentation maps. For each scene, we render 100 novel viewpoints in an orbital trajectory around the object to perform iterative segmentation lifting and Gaussian-object merging. Despite the challenging setting of using only 8 input training views, our method produces coherent and largely accurate segmentations, with only minor missegmentation in a few regions.

Sampled Views

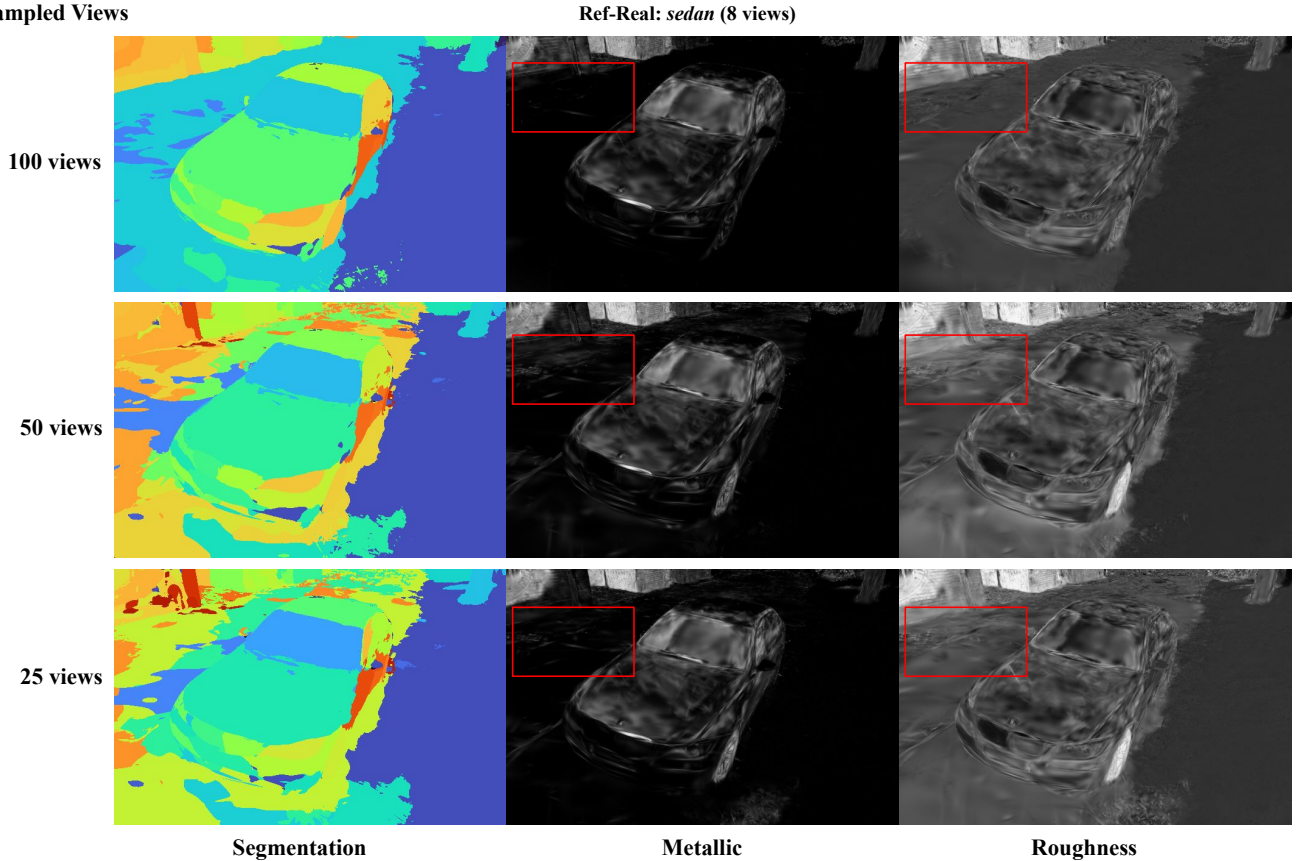


Figure 11. **Impact of the number of novel views used for the segmentation lifting and merging mechanism.** Each row presents the resulting segmentation render in column 1, the metallic map in column 2, and the roughness map in column 3. From top to bottom, we show results using 100, 50, and 25 novel views utilized for lifting and merging of gaussian objects. As the number of views decreases, some regions become noticeably over-segmented, leading to increased noise and irregularities in the estimated material properties, defeating the purpose of our proposed segmentation guidance. We also observe that the resulting segmentation consistency relies on the reconstructed geometry from stage 1, demonstrating that a sufficient shape estimation is crucial for material recovery.

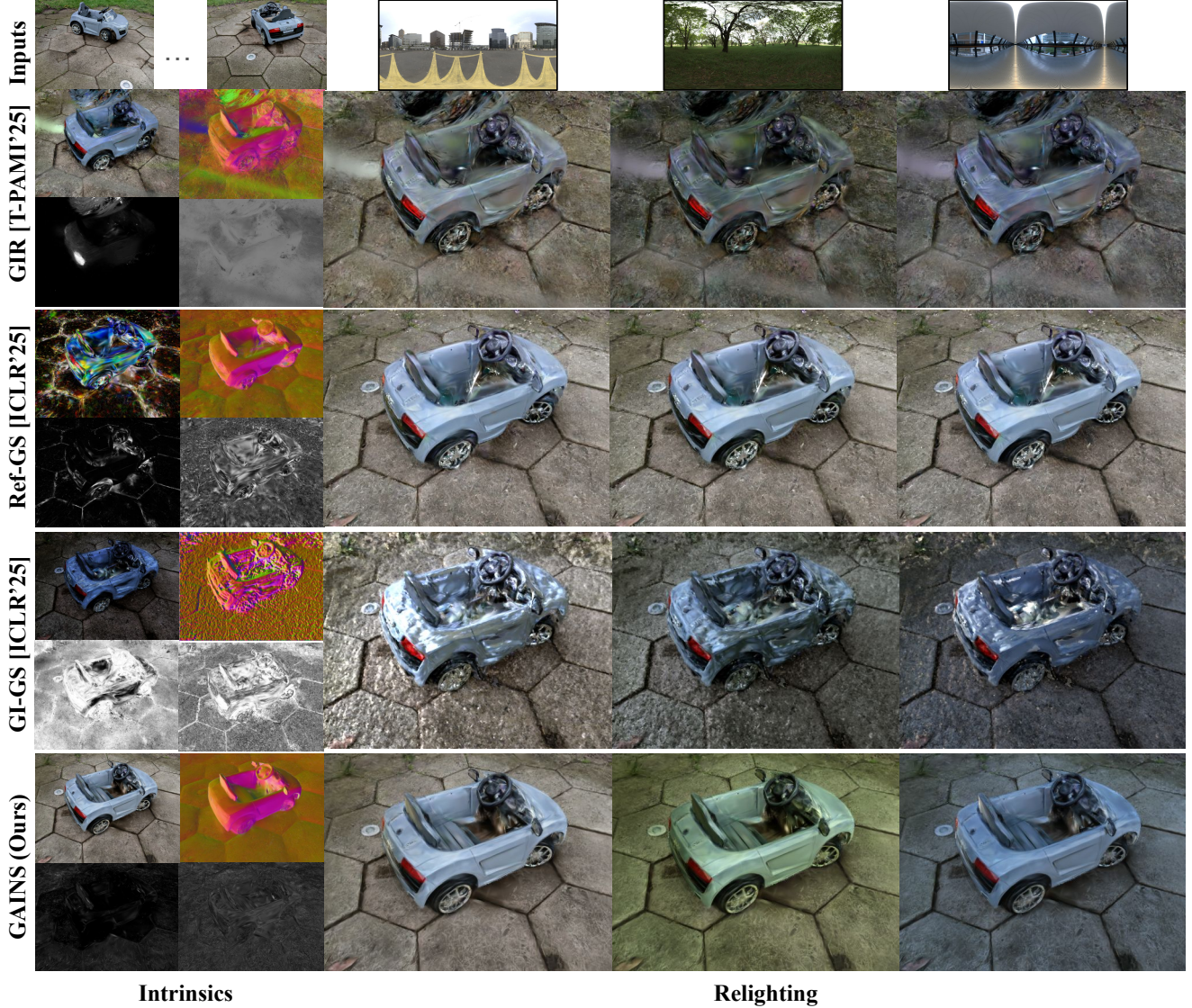


Figure 12. **Qualitative comparison of intrinsic estimation and relighting on the *sedan* scene from the Ref-Real dataset [29], reconstructed from 8 views.** The rows show results from top to bottom for: GIR [26], Ref-GS [36], GI-GS [3], and GAINS (Ours). Column 1 presents novel-view intrinsic renderings in a 2×2 layout: (top) albedo and surface normals, (bottom) specular roughness and metallic. Columns 2–4 show relighting results under three different novel environment maps. Across all lighting conditions, GAINS produces more stable and realistic relighting, consistent shading, and fewer artifacts. Our method also recovers more accurate and smoother surface normals, which directly improves shading behavior and enables physically meaningful relighting across viewpoints. The results further highlight the importance of high-quality geometry reconstruction. GAINS exhibits far less noise in the recovered material maps, yielding cleaner intrinsics and significantly more faithful relit appearances across all three environment maps.



Figure 13. **Qualitative comparison on the *toy car* scene trained with different numbers of input views (top: 4 views, bottom: 16 views).** Results for the 8-view setting are provided in Fig. 12. Each row corresponds to a method: GAINS (ours), Ref-GS, and GI-GS. The first column shows intrinsic predictions arranged in a 2×2 grid (top-left: albedo, top-right: normals, bottom-left: metallic, bottom-right: roughness), while the remaining columns show relighting under novel environment maps. Our method maintains accurate intrinsic reconstruction and stable relighting quality across all training-views, whereas baseline methods degrade noticeably, particularly under sparse inputs.

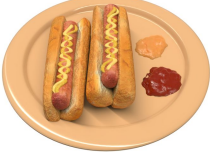
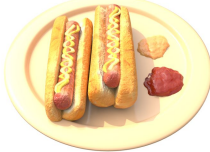

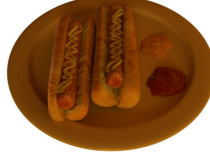
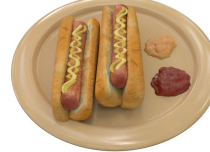





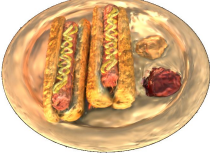




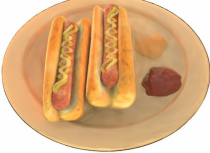




	Bridge	City	Courtyard	Fireplace	Forest
GT					
Ref-GS	 PSNR: 8.39 SSIM: 0.71 LPIPS: 0.255	 PSNR: 8.32 SSIM: 0.71 LPIPS: 0.255	 PSNR: 7.76 SSIM: 0.67 LPIPS: 0.27	 PSNR: 7.94 SSIM: 0.71 LPIPS: 0.29	 PSNR: 8.23 SSIM: 0.72 LPIPS: 0.277
GI-GS	 PSNR: 19.99 SSIM: 0.79 LPIPS: 0.185	 PSNR: 19.57 SSIM: 0.81 LPIPS: 0.185	 PSNR: 20.36 SSIM: 0.83 LPIPS: 0.166	 PSNR: 23.13 SSIM: 0.87 LPIPS: 0.15	 PSNR: 21.07 SSIM: 0.81 LPIPS: 0.16
Ours	 PSNR: 22.06 SSIM: 0.87 LPIPS: 0.115	 PSNR: 21.09 SSIM: 0.88 LPIPS: 0.131	 PSNR: 21.26 SSIM: 0.87 LPIPS: 0.116	 PSNR: 23.93 SSIM: 0.9 LPIPS: 0.111	 PSNR: 21.94 SSIM: 0.88 LPIPS: 0.12

Figure 14. **Relighting comparison across different lighting conditions on the *hotdog* scene from the TensoIR [10] dataset.** Each column shows different relighting results. Rows correspond to Ref-GS [36], GI-GS [3], and our method.

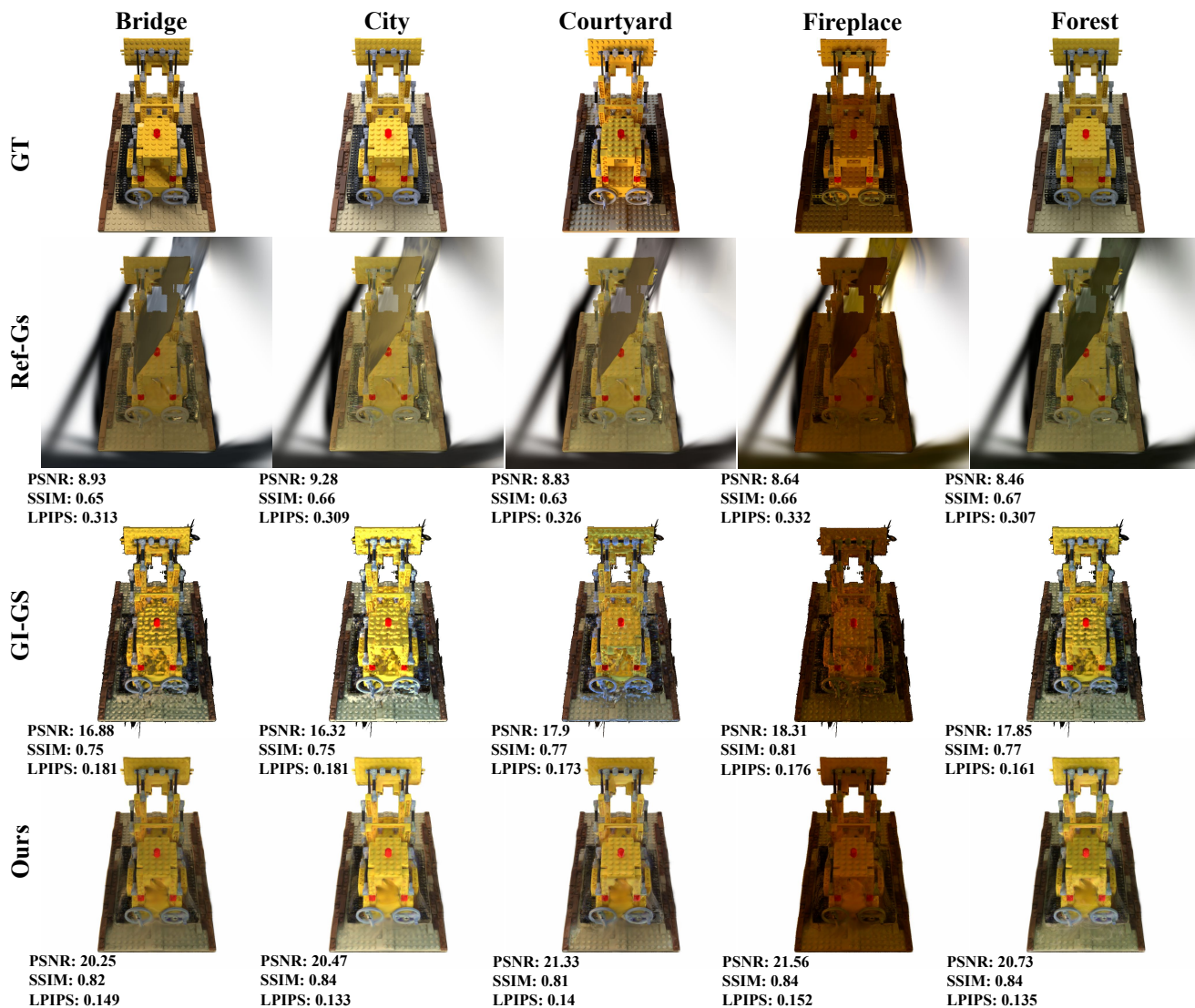


Figure 15. **Relighting comparison across different lighting conditions on the *lego* scene from the TensorIR [10] dataset.** Each column shows different relighting results. Rows correspond to Ref-GS [36], GI-GS [3], and our method.

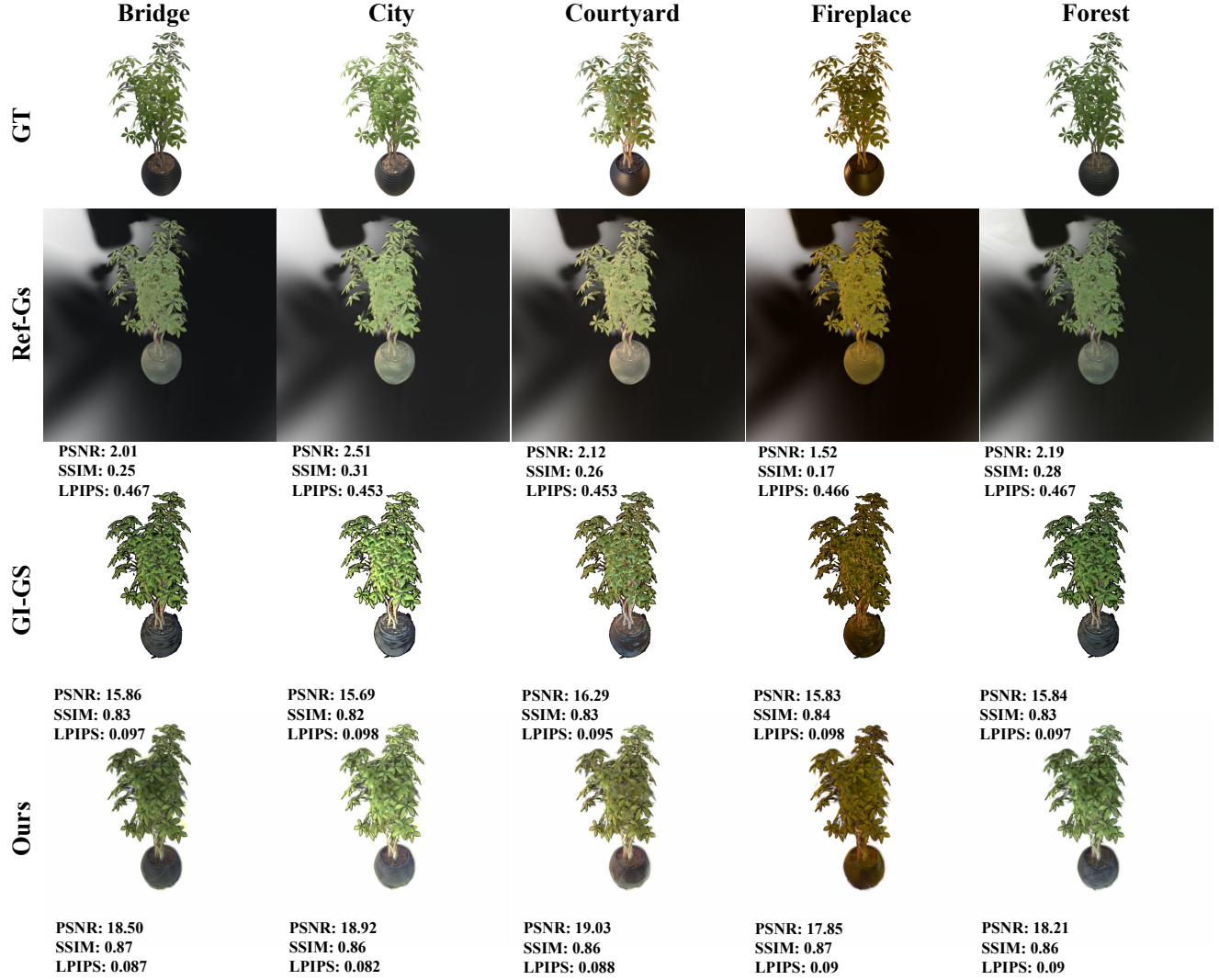


Figure 16. **Relighting comparison across different lighting conditions on the *ficus* scene from the TensoIR [10] dataset.** Each column shows different relighting results. Rows correspond to Ref-GS [36], GI-GS [3], and our method.





















	Bridge	City	Courtyard	Fireplace	Forest
GT					
Ref-Gs					
	PSNR: 26.03 SSIM: 0.94 LPIPS: 0.076	PSNR: 26.62 SSIM: 0.94 LPIPS: 0.074	PSNR: 26.51 SSIM: 0.92 LPIPS: 0.08	PSNR: 25.27 SSIM: 0.93 LPIPS: 0.076	PSNR: 27.20 SSIM: 0.95 LPIPS: 0.074
GI-GS					
	PSNR: 19.72 SSIM: 0.88 LPIPS: 0.106	PSNR: 19.17 SSIM: 0.86 LPIPS: 0.11	PSNR: 19.91 SSIM: 0.87 LPIPS: 0.107	PSNR: 19.82 SSIM: 0.90 LPIPS: 0.099	PSNR: 19.89 SSIM: 0.89 LPIPS: 0.103
Ours					
	PSNR: 24.43 SSIM: 0.92 LPIPS: 0.079	PSNR: 23.98 SSIM: 0.92 LPIPS: 0.078	PSNR: 25.02 SSIM: 0.91 LPIPS: 0.084	PSNR: 24.44 SSIM: 0.92 LPIPS: 0.081	PSNR: 24.09 SSIM: 0.92 LPIPS: 0.078

Figure 17. **Relighting comparison across different lighting conditions on the *armadillo* scene from the TensoIR [10] dataset.** Each column shows different relighting results. Rows correspond to Ref-GS [36], GI-GS [3], and our method.

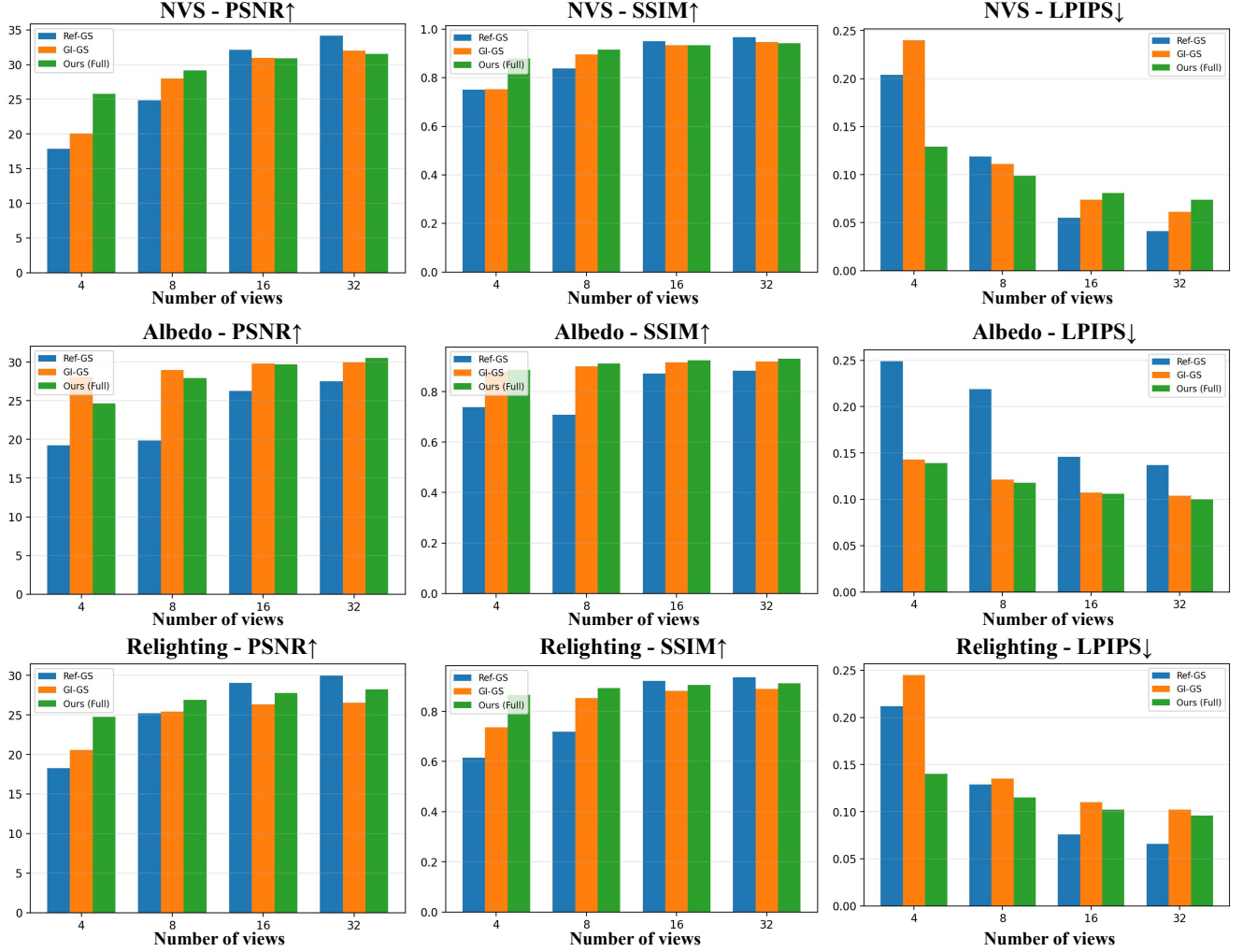


Figure 18. **Comparison of our method with Ref-GS [36] and GI-GS [3] on the TensoIR [10] dataset across increasing numbers of input views.** Columns (left to right) report PSNR, SSIM, and LPIPS. Rows correspond to novel-view synthesis (NVS), albedo estimation, and relighting. Each bar chart shows results for 4, 8, 16, and 32 input views, with blue indicating Ref-GS, orange indicating GI-GS, and green indicating GAINS (ours). GAINS consistently surpasses both baselines across all metrics in sparse-view settings (4–8 views) and remains competitive as the number of views increases.